

#### **Research Article**

Yi Zhang and Jinli Huang\*

# Structure of the Sediment and Crust in the Northeast North China Craton from Improved Sequential H-k Stacking Method

https://doi.org/10.1515/geo-2019-0054 Received Mar 03, 2019; accepted Jun 28, 2019

Abstract: H-k stacking method is a standard receiverfunction method to detect crustal thickness. But this method can not be applied in low-velocity sedimentary basins. To solve this problem, we propose an improved sequential H-k stacking method. The improved method needs two sequential stacks. Firstly, sediment structure is calculated using converted waves and multiples on the bottom boundary of sediments. Secondly, the sedimentary results are applied to calculate the crustal structure. Theoretical calculations and "recovery tests" indicate that the improved method can obtain accurate estimates in sedimentary basins. With the teleseismic data of North China Craton, the structure of sediments is thick in the depression and thin in the uplifted area, which is consistent with Deep Seismic Sounding results. The crust to the west of the North-South Gravity Lineament is relatively thick and has a low average Poisson ratio, whereas the east is relatively thin and has a high average Poisson ratio. This result and the structural feature from data regression imply that the eastern crust of the North China Craton has experienced wide extension, which reflect the crustal response to the severe destruction and deformation in that area compared to the western crust.

**Keywords:** Improved sequential H-k stacking method, Sediment and crustal structure, North China Craton

#### 1 Introduction

North China was one of the oldest cratonic areas. The unified continental craton was formed through the continentcontinent collision between the eastern blocks (EB) and western blocks (WB) of the North China Craton (NCC) along the Trans-North China Orogen (TNCO) at ~1.8 Ga (Figure 1) [1]. The NCC remained stable from the Mesoproterozoic to the early Triassic. Beginning in the Mesozoic, large-scale deformation and magmatic events occurred, including lithospheric thinning and intensive crustal extension [2–5]. The study area is located in the northeast NCC and is composed of the Yanshan uplift area (YU), the Taihang Mountains (TM), and the North China Basin (NCB) (Figure 1). Most of our study area is on the EB and TNCO, which has experienced obvious destruction and deformation (Figure 1). Therefore, this area is the key to understanding the destruction process of the NCC. We can investigate the crustal structure and the crustal response to regional extension by using seismic data from the dense seismic stations distributed in this area (Figure 1), thus providing significant constraints on the destruction process of the NCC.

The receiver function method can efficiently detect significant discontinuity structures in the deep earth by using converted waves generated on discontinuities (e.g., the Moho, the bottom boundary of the lithosphere and the discontinuity of the upper mantle) [1, 6–8]. Zhu and Kanamori [9] proposed the H-k stacking method to obtain crustal thickness and the Poisson ratio. This method was applied by many scientists in studies of the NCC and obtained significant results [10, 11]. Chen et al. [12] applied a receiver function poststack migration method to image the crustal and upper mantle structures beneath the NCC. To eliminate the effect of thick sediments, they used the PpPs multiples instead of the commonly used Ps converted phases to image the Moho discontinuity. Tang et al. [13] extended the H-k stacking method of receiver functions applicable to a three layer model and applied this method to two sample sites in Taiwan. Wei et al. [14] investigated



<sup>\*</sup>Corresponding Author: Jinli Huang: School of Geophysics and Information Technology, China University of Geosciences, Beijing, 100083, China; Email: huangil@cugb.edu.cn

**Yi Zhang:** Key Laboratory of Geo-detection (China University of Geosciences, Beijing), Ministry of Education, 100083, China 2 School of Geophysics and Information Technology, China University of Geosciences, Beijing, 100083, China

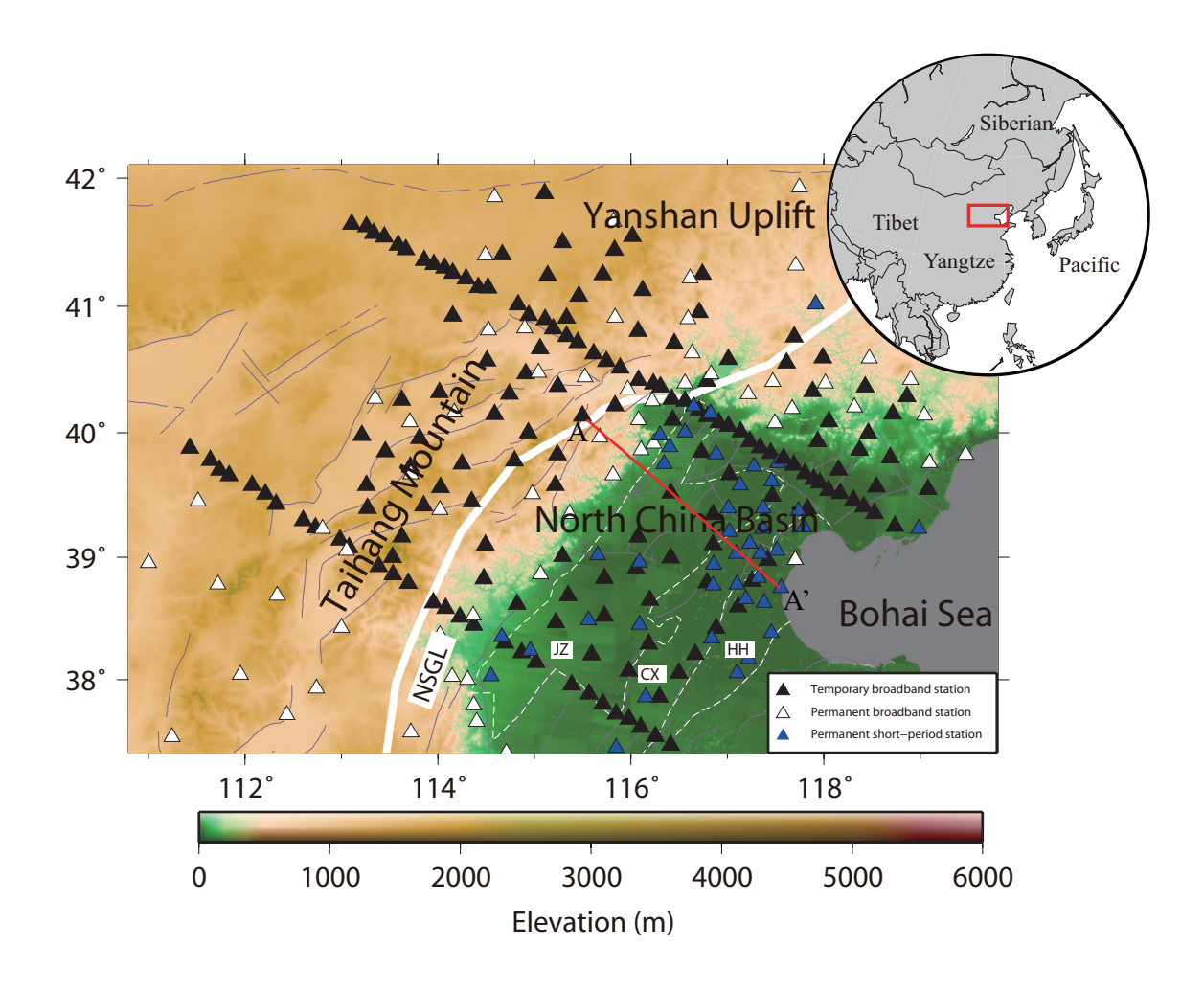


Figure 1: Seismic station distribution of the study area.

The distribution of seismic stations. The black triangles represent broadband temporary stations, the white triangles represent broadband permanent stations, the blue triangles represent short-period permanent stations, the colored background indicates topography, and the thin gray lines represent major faults. Three major secondary structural units are delineated using dashed white lines: the Jizhong depression (JZ), Cangxian uplift area (CX), and Huanghua depression (HH). The red line indicates the location of the DSS profile (AA') shown in Figure 8, and the thick white lines in both figures represent North-South Gravity Lineament (NSGL). The red rectangle in the upper-tight

crustal thickness and the Poisson ratio of east China using H-k stacking method, but they only used the data from broadband stations. The disadvantage of the above studies was that they did not use the data from seismic stations in the sedimentary area. Because there were thick sediments covering the basin and the sediment multiples could disturb the travel times of Moho multiples, H-k stacking method would be invalid due to its large errors in estimates of Moho depth.

map represents the location of the whole research area.

To correct the effect of the sedimentary basins, many scientists proposed their solutions. With the regional earthquake events, Kennett developed a P-SV decomposition method and employed specific slowness band approximations to obtain the relative contributions of P, SV and SH waves [15]. His approach showed a relatively simple and effective procedure to correct the effect of the surface. William *et al.* [16] proposed a sequential H-k stacking method. This method had two sequential stacks. In the first stack, the P-wave velocity of sediments was assumed to calculate the thickness and Vp/Vs ratio of sediments. In the second stack, the thickness and Vp/Vs ratio of crust were obtained by using the results of sediments. Although this method could obtain the sediment and crustal structure in sedimentary area, they used an assumed P-wave velocity which could result in a significant error in the calculation of the sediment thickness. That error in-

creased when the sediments became thicker and thereby propagated into the calculation of crustal thickness. Tao et al. [17] proposed that the receiver function could be treated as the stacking of converted waves from several layers. By separating those waves from the receiver functions, they could obtain the thickness and Vp/Vs ratio of sediments and crust. However, the assumption must be made that the upcoming wave from the teleseism excludes S-wave information to calculate the optimized layer coefficient solution. Yu et al. [18] used the auto-correlation method on the observed receiver functions to determine the strength and two-way travel-time of the reverberations. Then they constructed a resonance removal filter in the frequency domain to remove the sediment reverberations and deciphered the Ps phases associated with the Moho discontinuity.

For the thick sediments in the east part of NCC, we propose an improved sequential H-k stacking method based on the previous H-k stacking methods. This improved method needs two sequential stacks. The thickness and wave velocity of sediments are obtained in the first stack, and the thickness and Vp/Vs ratio of crust are estimated in the second stack by using sediment result. Through two sequential stacks, we can obtain the structure of sediments and crust in sedimentary areas. In this study, we still use the H-k stacking method in the TM and YU. Moreover, the improved method is applied in the NCB with sediments. By comprehensively using data from broadband and shortperiod seismic stations, we do not only obtain distributions of crustal thickness and Poisson ratio over the entire study area but also the thickness distribution of the sediments in the NCB to provide more detailed information on the crustal structure.

#### 2 Data and Method

#### 2.1 Data

The data used in this study includes teleseismic waves from permanent seismic stations run by China Earthquake Administration, and from North China temporary stations employed by the Institute of Geophysics, China Earthquake Administration [19]. A total of 291 seismic stations are used in this study, 249 of which are broadband stations and 42 of which are short-period stations (Figure 1). Teleseismic waves are selected from earthquakes events for all  $M_L > 5.5$  earthquakes from November 2006 to July 2009 with epicentral distances between 30° and 90° (Figure 2), from which 6027 receiver functions are obtained.

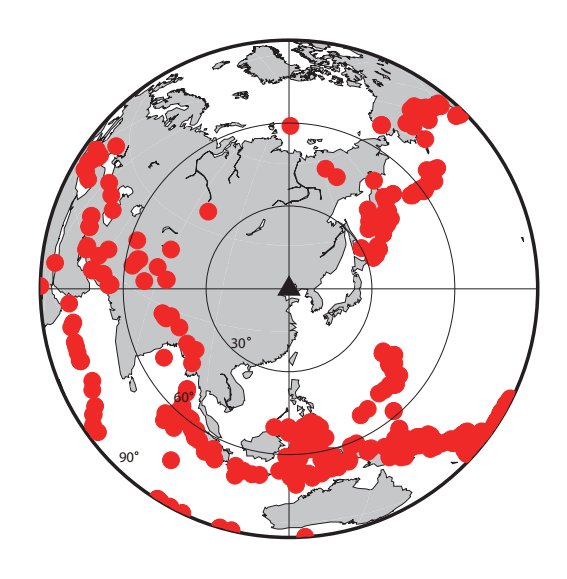


Figure 2: Distribution of the teleseismic events used in this study. In this figure, the red points mark the epicentral positions of the teleseismic events used in this study. The black triangle indicates the center of the study area ( $115^{\circ}E$ ,  $40^{\circ}N$ ). The numbers on the concentric circles— $30^{\circ}$ ,  $60^{\circ}$ , and  $90^{\circ}$ —are epicentral distances.

In this research, we use the iterative time-domain deconvolution method to extract the receiver functions [20]. Compared to the frequency-domain method, the time-domain method is free of complex relationships between water-level values and damping parameters. Meanwhile, the time-domain method does not suffer the "acausal trough" surrounding the P wave arrival that decreases the ampliude of the first few arrivals. The receiver functions estimated by time-domain method can reserve more details of the sedimentary basins. For short-period stations, the teleseismic waves are pretreated first. According to the proposed method by Niu *et al.* [21], the instrument responses of short-period stations can be treated as high-pass filters:

$$I(w) = \frac{Gw^2}{-w^2 + 2ihw_0 + w_0^2} \tag{1}$$

where  $w_0$  is a frequency constant, h is a damping constant, and G is a gain factor. Seismic waves are received by short-period stations with suppressed low-frequency components, which is equivalent to a high-pass filters. Thus, to recover the low-frequency components, teleseismic waves from short-period stations must use deconvolution to remove the instrumental response.

#### 2.2 Method

Zhu and Kanamori [9] have proposed the H-k stacking method. The basic idea of this method is to utilize the converted wave (Ps) and the multiples (PpPs, PpSs+PsPs) on the Moho to determine the thickness H and Vp/Vs ratio k of crust under the station. But The H-k stacking method can generate large errors in sedimentary basins. The presence of low-velocity sedimentary basins causes a delay of arrivals from deeper converters such as the crust-mantle boundary (Moho), which leads to incorrect mapping of the Moho. Reverberating phases (multiple waves) in the sediment layer may also overprint Moho arrivals. These complexities make it difficult to resolve Moho depth of the receiver functions in sedimentary basins. To address that problem, William et al. [16] have proposed a sequential Hk stacking method. The method employs two sequential stacks. In the first stack, the thickness and Vp/Vs ratio of the sediments are determined by using the converted wave  $Ps_{(sed)}$ ,  $PpPs_{(sed)}$  and  $PpSs+PsPs_{(sed)}$  multiples on the bottom boundary of sediments. In the second stack, the results of sediments are substituted to calculate crustal thickness H and Vp/Vs ratio k. In the sequential H-k stacking method, the thickness and Vp/Vs ratio of sediments are first calculated with the assumed sediment P-wave velocity. Then, the thickness and Vp/Vs ratio of the crust are calculated by using the results of sediments (thickness and Vp/Vs ratio). Due to the large range of sediment velocities  $V_{n(sed)}$ , there can be large discrepancies between the assumed sediment velocity  $V_{p(sed)}$  and the actual velocity in the first stack, which will result in large errors in the results of the sediments and crust.

To address the problem of the previous methods, we propose an improved sequential H-k stacking method. If the effect of the assumed sediment P-wave velocity is removed, we can obtain the P-wave travel time and Vp/Vs ratio with more precision. Then the thickness of sediments is calculated using more accurate P-wave velocity from Deep Seimic Sound (DSS) or borehole result. Considering the relatively low seismic wave velocities in sediments, teleseismic rays are perpendicularly incident to the surface after passing through sediments; that is, the incident angle  $\theta$  is very small and equivalent to ray parameter p = 0 $(p = \sin(\theta)/V)$ . We therefore suppose in this method that ray parameter p = 0, indicating that our assumption is consistent with the actual situation. The reason for assuming the ray parameter p = 0 is that the P-wave velocity is bound to ray parameter (Equation 3), and the term of P-wave velocity can be eliminated after the assumption. This fact will be verified by our calculation results in the following sections. The sediment Vp/Vs ratio  $(k_{(sed)})$  and the travel

time of a P-wave in the sediments  $(T_{(sed)})$  are calculated as follows.

the relationships between sediment thickness  $H_{(sed)}$  and the travel times of the converted wave  $(t_{Ps(sed)}, t_{PpPs(sed)},$  and  $t_{PsPs+PpSs(sed)})$  can be expressed as.

$$H_{(sed)} = \frac{t_{Ps(sed)}}{\sqrt{\frac{1}{V_{s(sed)}^2} - p^2} - \sqrt{\frac{1}{V_{p(sed)}^2} - p^2}}$$

$$H_{(sed)} = \frac{t_{PpPs(sed)}}{\sqrt{\frac{1}{V_{s(sed)}^2} - p^2} - \sqrt{\frac{1}{V_{p(sed)}^2} - p^2}}$$

$$H_{(sed)} = \frac{t_{PpSs+PsPs(sed)}}{2\sqrt{\frac{1}{V_{s(sed)}^2} - p^2}}$$
(2)

If we substitute  $k_{(sed)} = V_{p(sed)}/V_{s(sed)}$  into Equation (2), and transform the left side of the Equation (2) to k(sed):

$$k_{(sed)} = (3)$$

$$\sqrt{\left(\frac{V_{p(sed)}t_{Ps(sed)}}{H_{(sed)}} + \sqrt{1 - V_{p(sed)}^{2}p^{2}}\right)^{2} + V_{p(sed)}^{2}p^{2}}$$

$$k_{(sed)} = \sqrt{\left(\frac{V_{p(sed)}t_{PpPs(sed)}}{H_{(sed)}} + \sqrt{1 - V_{p(sed)}^{2}p^{2}}\right)^{2} + V_{p(sed)}^{2}p^{2}}$$

$$k_{(sed)} = \sqrt{\left(\frac{V_{p(sed)}t_{PpSs+PsPs(sed)}}{2H_{(sed)}}\right)^{2} + V_{p(sed)}^{2}p^{2}}$$

Because the teleseismic ray is incident perpendicular to the surface, the travel time of the P-wave in the sediments can be expressed as  $T_{(sed)} = H_{(sed)}/V_{p(sed)}$  and substituted into Equation (3):

$$k_{(sed)} = \frac{t_{Ps(sed)}}{T_{(sed)}} + 1,$$
 (4)

$$k_{(sed)} = \frac{t_{PpPs(sed)}}{T_{(sed)}} - 1, \tag{5}$$

$$k_{(sed)} = \frac{t_{PpSs+PsPs(sed)}}{2T_{(sed)}}. (6)$$

we can define the target function as,

$$s\left(T_{(sed)}, k_{(sed)}\right) = w_1 r\left(t_{Ps(sed)}\right) + w_2 r\left(t_{PpPs(sed)}\right)$$
(7)  
+  $w_3 r(t_{PpSs+PsPs(sed)})$ 

where r is amplitude and  $w_1$ ,  $w_2$ , and  $w_3$  are the weighted coefficients that correspond to seismic phase  $Ps_{(sed)}$ ,  $PpPs_{(sed)}$ , and  $PpSs + PsPs_{(sed)}$ , respectively, which sum to 1. The maximum value of  $s(T_{(sed)}, k_{(sed)})$  and the corresponding travel time  $T_{(sed)}$  of P-wave and Vp/Vs ratio  $k_{(sed)}$  can be determined by grid searching upon substituting Equations (4), (5) and (6) into Equation (7). In the

second stack, the travel time  $T_{(sed)}$  obtained from the first stack is utilized to convert the sediment thickness  $H_{(sed)}$ . Then,  $H_{(sed)}$  and  $k_{(sed)}$  are used to estimate the thickness and Vp/Vs ratio of crust [16]

$$t_{PS} = (H - H_{(sed)})$$

$$\star \left( \sqrt{\frac{1}{V_s^2} - p^2} - \sqrt{\frac{1}{V_p^2} - p^2} \right) + T_{(sed)}$$

$$\star (k_{(sed)} - 1)$$

$$t_{PpPS} = (H - H_{(sed)}) \star \left( \sqrt{\frac{1}{V_s^2} - p^2} - \sqrt{\frac{1}{V_p^2} - p^2} \right)$$

$$+ T_{(sed)} \star (k_{(sed)} + 1)$$

$$t_{PSPS+PpSS} = 2 \star (H - H_{(sed)}) \star \left( \sqrt{\frac{1}{V_s^2} - p^2} \right)$$

$$+ 2T_{(sed)}k_{(sed)}$$

where H is the crustal thickness, the Vs and Vp are the crustal S and P wave velocity respectively, and the  $t_{Ps}$ ,  $t_{PpPs}$ , and  $t_{PsPs+PpSs}$  are the travel times of the converted waves from Moho discontinuity. With the equation (8), the resulting H-k stack is corrected for sediment effects. From above calculation process, we can see that the improved method does not need the assumption of the sediment P-wave velocity  $V_{p(sed)}$  when calculating  $T_{(sed)}$  and  $k_{(sed)}$ , which is different from the sequential H-k stacking method. Then the more accurate  $H_{(sed)}$  can be calculated from the Pwave velocity from DSS or borehole result. Thus, the Vp/Vs ratio  $k_{(sed)}$  avoids the effect from  $V_{p(sed)}$ , which thereby improves calculation precision. Although the ray parameter p is set to 0, it is consistent with the actual situation of sedimentary basins and leads to insignificant errors. In the next section, a detailed error analysis of the method proposed in this study is discussed.

### 2.3 Error analysis of the improved sequential H-k stacking method

#### 2.3.1 Error from assumption

In the improved sequential H-k stacking method, we assume that ray parameter p=0. Next, we analyze the errors caused by this assumption. To that end, we use the Taylor series expansion on Equation (2) at point p=0. In the expansion expression, the first order terms of p is  $\frac{\partial k_{(sed)}}{\partial p}$  = 0, and we keep the second order terms. The expression  $T_{(sed)} = H_{(sed)}/V_{p(sed)}$  is substituted to obtain the following equations:

$$k_{(sed)} = \frac{t_{PS(sed)}}{T_{(sed)}} + 1 - \frac{t_{PS(sed)}V_{p(sed)}^2p^2}{2(t_{PS(sed)} + T_{(sed)})} + e_{12}, \quad (9)$$

$$k_{(sed)} = \frac{t_{PpPs(sed)}}{T_{(sed)}} - 1 + \frac{t_{PpPs(sed)}V_{p(sed)}^2p^2}{2(t_{PpPs(sed)} + T_{(sed)})} + e_{22}, \quad (10)$$

and

$$k_{(sed)} = \frac{t_{PpSs+PsPs(sed)}}{2T_{(sed)}} + \frac{T_{(sed)}V_{p(sed)}^2p^2}{(t_{PpSs+PsPs(sed)})} + e_{32}$$
 (11)

In the above equations,  $e_{12}$ ,  $e_{22}$  and  $e_{32}$  represent the sums of the terms higher than second order, which can be ignored because their values are smaller than the second order terms by an order of magnitude. Comparing the Taylor expansion expressions (9)-(11) with the original Equations (4)-(6) under the assumption of p=0, the comparisons indicate that the error resulting from the assumption is mainly the second order term. Therefore, we quantify the error by substituting the regular sedimentary model parameters in the following discussion.

Assume the sediment layer is a horizontal monolayer model with a thickness of 3 km, Vp of 3km/s, Vp/Vs ratio of 3, and ray parameter of 0.07 [22]. We substitute these parameters into Equations (9)-(11) and obtain the second order terms in Equation (12):

$$\frac{t_{Ps(sed)}V_{p(sed)}^{2}p^{2}}{2\left(t_{Ps(sed)}+T_{(sed)}\right)} = 0.0147,$$

$$\frac{t_{PpPs(sed)}V_{p(sed)}^{2}p^{2}}{2\left(t_{PpPs(sed)}+T_{(sed)}\right)} = 0.0176,$$
and
$$\frac{T_{(sed)}V_{p(sed)}^{2}p^{2}}{\left(t_{PpSs+PsPs(sed)}\right)} = 0.0074.$$

As a result, under the assumption of p=0, the errors of Vp/Vs ratio  $k_{(sed)}$  are 0.0147 ( $Ps_{(sed))}$ ), 0.0176 ( $PpPs_{(sed)}$ ) and 0.0074 ( $PpSs + PsPs_{(sed)}$ ), respectively. Substituting the errors into Equation (2), the errors in the sediment thickness  $H_{(sed)}$  are 0.022 km, 0.013 km, and 0.007 km, respectively. Thus, the error of the Vp/Vs ratio  $k_{(sed)}$  is less than 0.5%, and the error of the thickness of sediments  $H_{(sed)}$  is less than 0.8%, implying a small error from the assumption. In the next section, we detect the errors by using "recovery tests" of the crustal model with sediments.

#### 2.3.2 Error detection using "recovery tests"

To further determine the precision of the improved sequential H-k stacking method, we apply two common crustal models with either velocity jump (Figure 3a) or velocity gradient in sediments (Figure 3f) for "recovery tests". The receiver functions of both models are calculated through Computer Programs in Seismology (CPS) [22]. We obtain twenty-one receiver functions with Gaussian low-pass filter factor of 3, and the ray parameter from 0.04 to 0.08

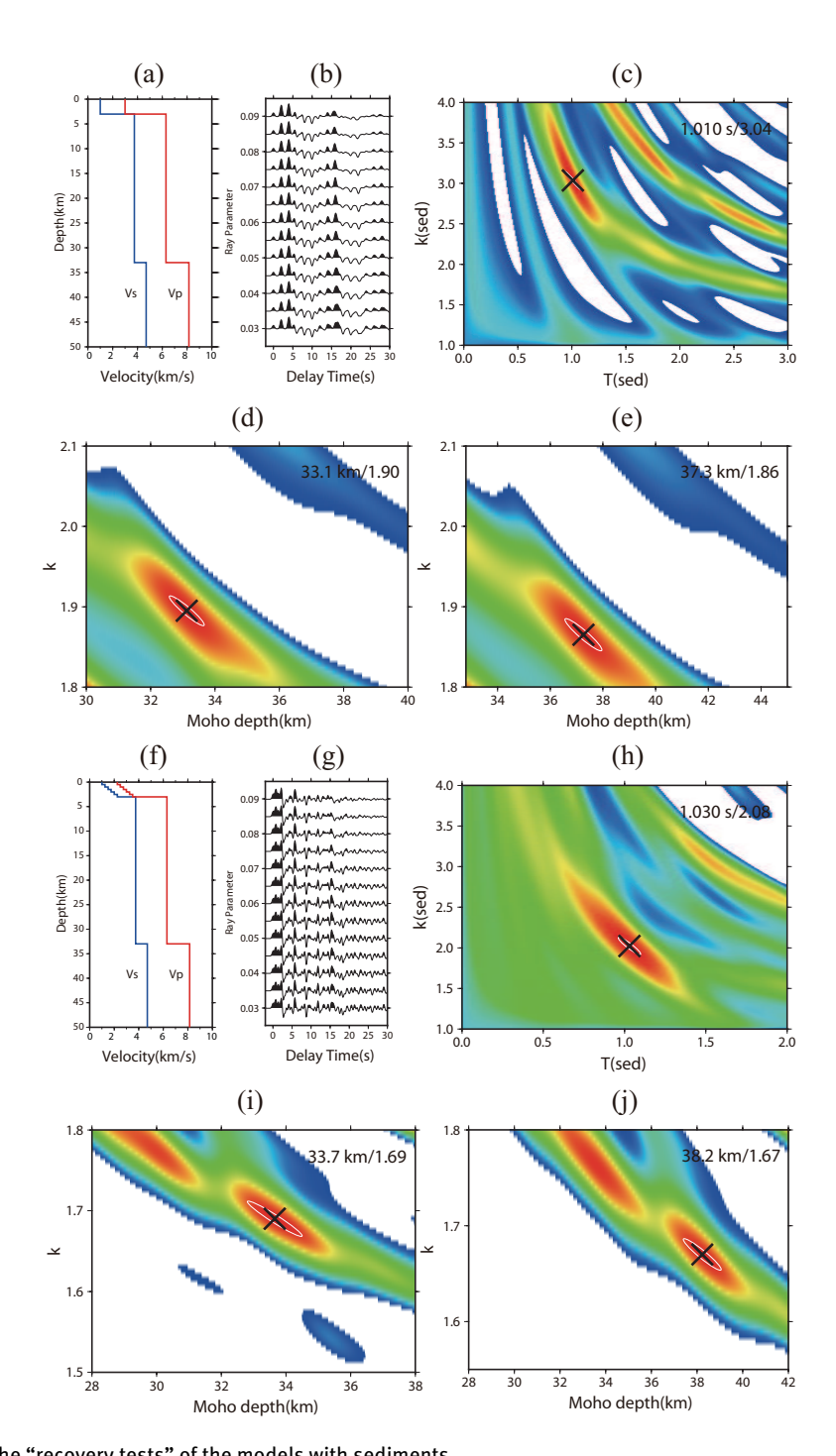


Figure 3: The results of the "recovery tests" of the models with sediments.

(a) and (f) represent the crustal models with velocity jump and velocity gradient in sediments, respectively. (b) and (g) are corresponding the theoretical receiver functions calculated by using the left velocity model. (c) and (h) are the results of the first stack by using the improved sequential H-k stacking method, in which the black crosses indicate the best estimate of the sediment P-wave travel time T(sed) and Vp/Vs ratio k(sed). The white circles represent the confidence. Due to the high confidence of the theoretical receiver functions, the white circles in (c) and (h) are too small to represent. (d) and (i) present the results of the second stack, in which the black crosses indicate the best estimate of the thickness and Vp/Vs ratio of crust. (e) and (j) are the results from the H-k stacking method, in which the black

crosses indicates the best estimate of the thickness and Vp/Vs ratio of crust.

by an interval of 0.005 (Figures 3b and 3g). The receiver functions from the forward calculation are utilized to obtain the thickness and Vp/Vs ratio of sediments and crust employing the improved sequential H-k stacking method (Figures 3c-d and Figures 3h-i). Comparing the results (Figures 3c-d, Figures 3h-i) with the corresponding input models (Figures 3a and 3f), we can see there are small errors by using the improved method. In addition, Figure 3e and Figure 3j also show the results from the H-k stacking method.

In the model with velocity jump in sediments (Figure 3a), assuming that the sediment thickness  $H_{(sed)} = 3$ km, P-wave velocity  $V_{(sed)} = 3$  km/s, and Vp/Vs ratio  $k_{(sed)}$  = 3, the Moho depth H=33 km, Vp=6.3 km/s, and Vs=3.75 km/s. The theoretical receiver functions are obtained through calculation (Figure 3b). By using the improved sequential H-k stacking method, the sediment Pwave travel time  $T_{(sed)} = 1.010 \text{ s}$  and Vp/Vs ratio  $k_{(sed)} =$ 3.04 are obtained from the first stack calculation (Figure 3c). Therefore, the corresponding sediment thickness is  $H_{(sed)} = T_{(sed)} * V_{p(sed)} = 3.03$  km. The crustal thickness obtained from the second stack is 33.1 km, and Vp/Vs ratio is 1.90 (Figure 3d). For the model with velocity jump in sediments, the comparison between the results from the improved sequential H-k stacking method and the theoretical values in input model ( $H_{(sed)} = 3 \text{ km}$ ,  $k_{(sed)} = 3$ , H=33 km, and k=1.909) indicates errors less than 1% for the thickness and Vp/Vs results of sediments. Compared to the theoretical thickness (33 km) and Vp/Vs ratio (1.909) of crust, the errors are 0.3% and 0.5%, respectively. Therefore, through the "recovery tests" of the model with velocity jump in sediments, the improved sequential H-k stacking method can accurately recover the model of hypothesis. For the crustal model with velocity jump in sediments (Figure 3a), the crustal thickness obtained from the H-k stacking method is 37.3 km and Vp/Vs ratio is 1.86 (Figure 3e). Compared to the theoretical values, the errors are 13% and 2.7%, respec-

In fact, the sediment in the basin usually has velocity gradient. Thus, we test the model with velocity gradient in sediments. The model is shown in Figure 3f. The surface velocities in this model are  $V_{p(sed)}=2.25~{\rm km/s}$  and  $V_{s(sed)}=1~{\rm km/s}$ . For every additional 0.5 km in depth,  $V_{p(sed)}$  and  $V_{s(sed)}$  each increase by 0.25 km/s, and  $H_{(sed)}=3~{\rm km}$ . All other parameters are similar to those of the previously discussed model. The theoretical receiver functions are obtained from CPS calculation (Figure 3g). With the improved method,  $T_{(sed)}=1.030~{\rm s}$  (corresponding to the sediment thickness  $H_{(sed)}=3.09~{\rm km}$ ) and  $k_{(sed)}=2.08$  (Figure 3h) are obtained from the first stack. Compared to the theoretical values ( $H_{(sed)}=3~{\rm km}$  and  $k_{(sed)}=2.12$ ), the errors are 3% and 1.8%, respectively. The crustal thick-

ness obtained from the second stack is 33.7 km, and the Vp/Vs ratio is 1.69 (Figure 3i). Compared to the theoretical values (H=33 km and k=1.761), the errors are 1.8% and 0.5%, respectively. For the model with velocity gradient in sediments (Figure 3f), the crustal thickness obtained from H-k stacking method is 38.2 km and the Vp/Vs ratio is 1.67 (Figure 3j). Compared to the theoretical values , the errors are 15.7% and 5.2%, respectively. The results show that in areas with thick sediments (*e.g.*, thickness more than 3 km), H-k stacking method is invalid for its significant error in crustal thickness. Thus, in such situations, the improved sequential H-k stacking method needs to be adopted.

#### 3 Results

When obtaining crustal structures with receiver functions stacking, we select different methods for two different situations. For the seismic stations in the NCB with sediments, we use the improved sequential H-k stacking method to obtain the sediment and crustal structures. For the TM and YU without sediments, we use the H-k stacking method [9].

#### 3.1 Sediment thickness results

Figure 4 shows the thicknesses of the sediments in the NCB obtained by using the improved sequential H-k stacking method. It is apparent that the sediments of the Jizhong depression are relatively thick, ranging from 2.9-6.7 km. The maximum thickness is 6.63 km, which occurs near Sanhe in the northern part of the Jizhong depression. Meanwhile, the sediments in the Cangxian uplift area become very thin (generally less than 2 km). The thinnest area is in southeast Tianjin in the northern Cangxian uplift area, where the thickness is 0.96 km. The thickness of the sediments increases again in the Huanghua depression at the southeastern edge of the NCB, and it is difficult to spatially restrict the variation in sediment thickness due to the small number of stations in the depression area. Yang and Huang [23] have used petroleum seismic velocity and results from DSS profiles to establish a high-precision 3D Pwave velocity model of the upper crust in the northeast of NCC. We select an average Vp(sed) of 3.5 km/s to calculate the sediment thickness [23, 24]. The variation trend of sediment thickness from the improved sequential H-k stacking method is consistent with the structural pattern (alternating uplift and depression) from previous work in the NCB area [23, 25, 26].

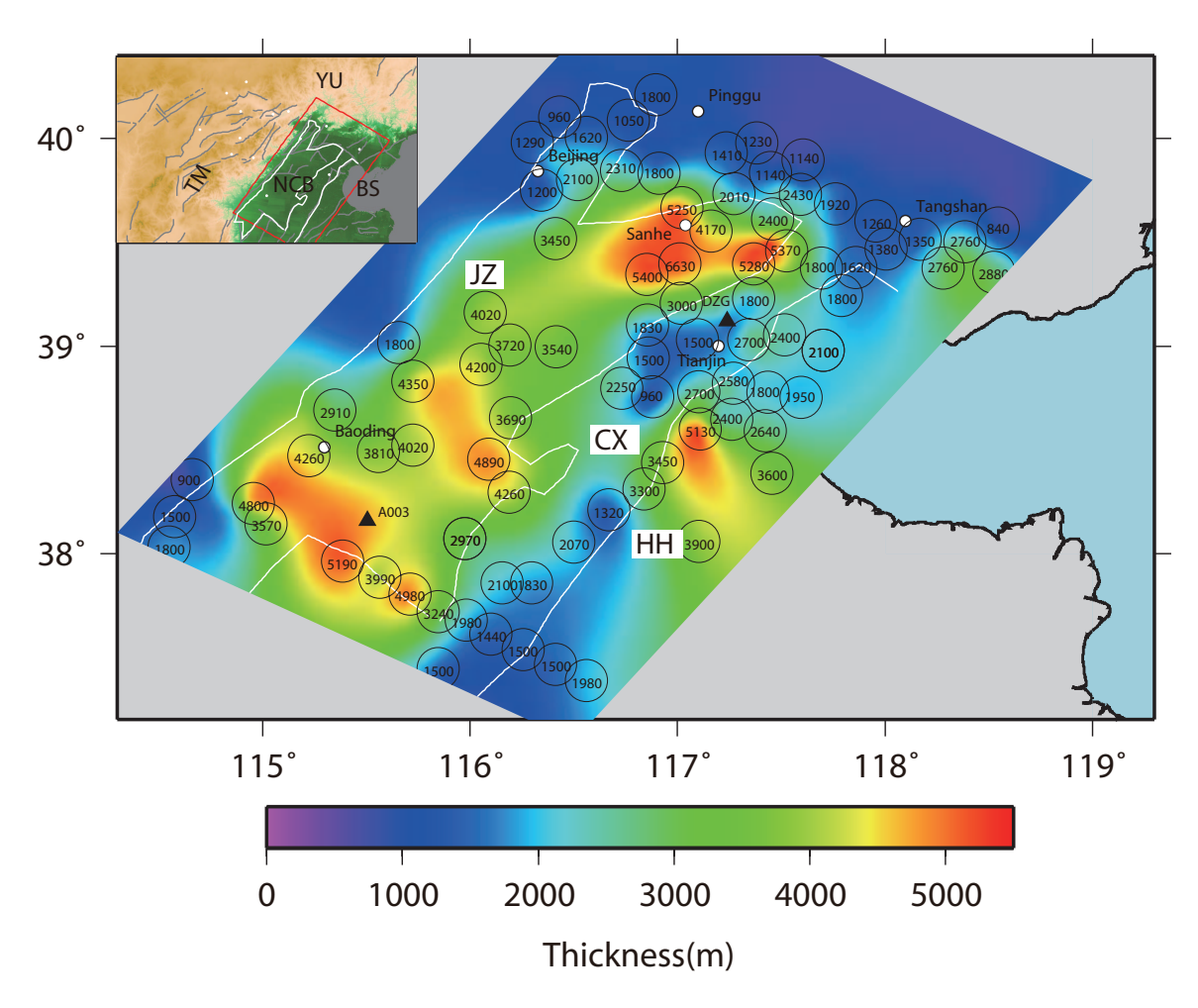


Figure 4: Sediment thickness in the NCB obtained by using the improved sequential H-k stacking method. The circles represent the stations used for sediment calculations. The numbers inside the circles represent the thickness of sediments under each station. The colors of the background show the distribution of the sediment thickness obtained through interpolation. The sediment thickness color scale is shown at the bottom. The white lines are the boundaries of sub-structural units that divide the NCB into the Jizhong depression (JZ), Cangxian uplift (CX), and Huanghua depression (HH). The black triangles indicate the locations of the two example stations that are shown in Figure 7 and are labeled with their corresponding names and sediment thickness. The red rectangle in the insert map at the upper-left corner shows the region where the sediment thickness was obtained.

#### 3.2 Crustal thickness results

Figure 5 shows the distribution of the crustal thickness in the study area. In the NCB with sediments, the results are obtained by using the improved sequential H-k stacking method. Whereas in the TM and YU without sediments, the results are estimated by using the H-k stacking method. Our results show that the crustal thickness changes from about 40 km in the west to 30 km in the east, gradually becoming shallow in general. From TM to NCB, there is a abrupt change belt of crustal thickness near NSGL, where the crustal thickness decreases rapidly from 40 km in the west to 35 km in the east. The average crustal thickness on the west side of NSGL is 38 km, and that on the east side is

32 km. The DSS profiles [25, 27] show that the crustal thickness of the TM and the western part of the YU ranges from 38 km to 42 km and that the crustal thickness of the NCB and the eastern part of YU ranges from 28 km to 34 km. Our results are consistent with the trend of crustal thickness variation from DSS profiles. Moreover, the Bouguer gravity anomaly map [28] indicates that the minimum gravity anomaly is located in the northwest TM and the maximum anomaly is located near Tianjin. In general, the Bouguer gravity anomaly increases from west to east. The regional gravity anomaly varies rapidly from –150 mgal on the west of NSGL to –90 mgal on the east. The variation of crustal thickness in this study (Figure 5) is identical to the trend of the gravity anomaly variation.

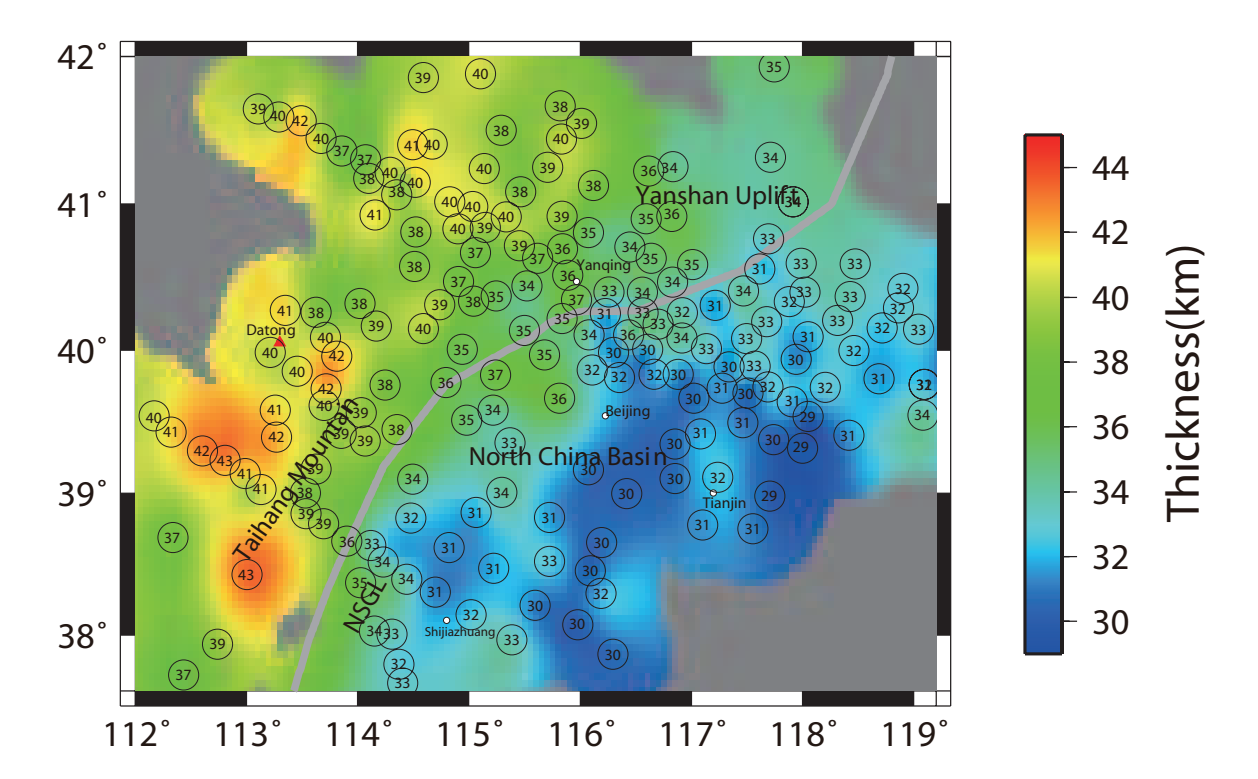


Figure 5: Distribution of crustal thickness in the study area.

The circles indicate the stations used for the crustal thickness calculations. The numbers inside the circles represent the corresponding crustal thickness under the stations. The background colors represent the distribution of crustal thickness obtained from interpolation. The red triangle shows the Datong volcano. The crustal thickness color scale is shown on the right. Other symbols are the same as those in Figure 1.

#### 3.3 Poisson ratio

As shown in Figure 6, except for some local areas with extremely high Poisson ratio, the Poisson ratio in most of the study areas ranges from 0.24-0.28, with an average of 0.27. A significant discrepancy of the Poisson ratio is found between the west and east sides of the NSGL. On the west of NSGL, the average Poisson ratio is 0.26 and the minimum value is 0.23. Whereas on the east of NSGL, the average Poisson ratio is as high as 0.28. There are two locations with high Poisson ratio anomalies. One is located near Datong volcano, and the other is located around Beijing. The maximum Poisson ratio in those two places is bigger than 0.32.

#### 4 Discussion

## 4.1 Comparison of the results between improved sequential H-k stacking method and other methods

Two typical seismic stations are selected here as examples to compare the results obtained by using two different H-k stacking methods (the H-k stacking method and the improved sequential H-k stacking method proposed in this paper) under conditions of different sediment thickness.

The DZG station is located in the Cangxian uplift area where covers thin sediments. The sediment thickness is approximately 2.4 km (Figure 4) and the crustal thickness is 33.0 km (Figure 7c) from the improved sequential H-k stacking method, whereas the crustal thickness is 33.7 km (Figure 7d) from the H-k stacking method. The crustal thickness is determined to be 30-32 km from DSS profiles near this station [25]. Considering the result of DSS profiles is more accurate, we use an average crustal thickness of 31 km as the reference value of the crustal thickness. The ab-

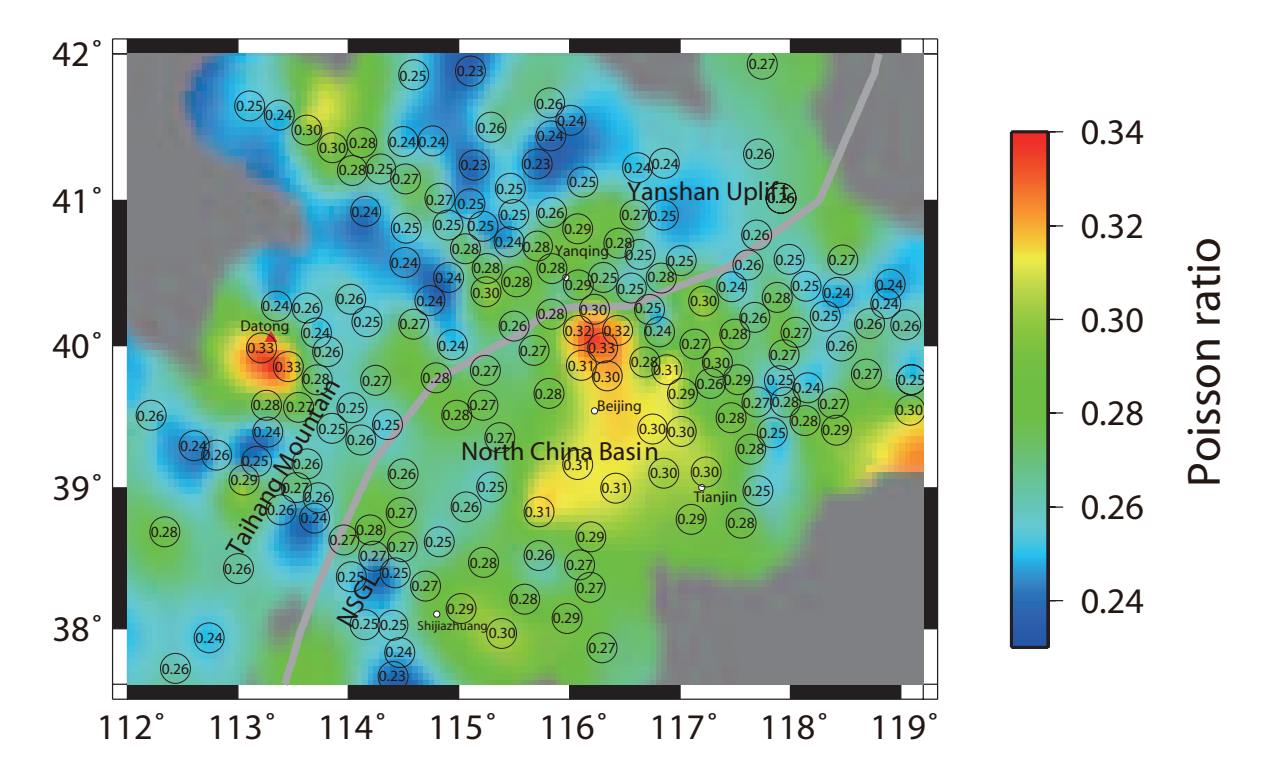


Figure 6: Distribution of crustal Poisson ratio in the study area.

The circles show the locations of the stations used to calculate the crustal Poisson ratio. The numbers inside the circles are the corresponding crustal Poisson ratio in this station. The background colors represent the distribution of the Poisson ratio obtained from interpolation. The red triangle shows the Datong volcano. The crustal Poisson ratio color scale is shown on the right. Other symbols are the same as those in Figure 1.

solute errors of the results from the improved sequential H-k stacking method and H-k stacking method are 2 km and 2.7 km, respectively, and the relative errors are 6.4% and 8.7%, respectively.

The A003 station is located in the Jizhong depression where covers thick sediments. The sediment thickness under this station is 4.2 km (Figure 4) and the crustal thickness is 30.1 km (Figure 7g) from the improved sequential H-k stacking method. On the other hand, the crustal thickness is estimated to be 33.9 km (Figure 7h) from the H-k stacking method. Employing the result of DSS profiles, the crustal thickness is 29 km near this station [25] and we use this value of 29 km as the reference value of the crustal thickness. The absolute errors of the results from the improved sequential H-k stacking method and H-k stacking method are 1.1 km and 4.9 km, respectively, and the relative errors are 3.8% and 16.9%, respectively.

According to the above results, it is demonstrated that the results from the improved method are closer to the reference values from DSS profiles and have higher precision compared to the results from the H-k stacking method in the areas where cover thick sediments. In addition, with increasing sediment thickness, the crustal thickness error from the H-k stacking method increases rapidly. For a sediment thickness of 2.4 km, the relative error from the H-k stacking method is 8.7%. When the sediment thickness increases to 4.3 km, the relative error increases to 16.9%. In contrast, the relative errors from the improved sequential H-k stacking method are between 3.2-3.8% with increasing sediment thickness. Thus, when the sediment thickness is thicker than 2 km, the results of crustal thickness from the H-k stacking method will be invalid due to the large errors. Instead, the improved sequential H-k stacking method proposed in this study needs to be applied in such situations.

To further illustrate the precision of the improved sequential H-k stacking method, we compare our results to the values obtained by the DSS profile (Figure 8) [25]. For the results from the DSS profiles, the 5.5 km/s and 7 km/s velocity contours are approximately equivalent to the bottom boundaries of the sediments and crust (the green solid line in Figure 8). Thus, the sediment and crustal thickness from the improved method are mostly identical to the DSS results, except a little discrepancy when crossing the thick sediments at about  $116.5^{\circ}E$ . The reason of this discrep-

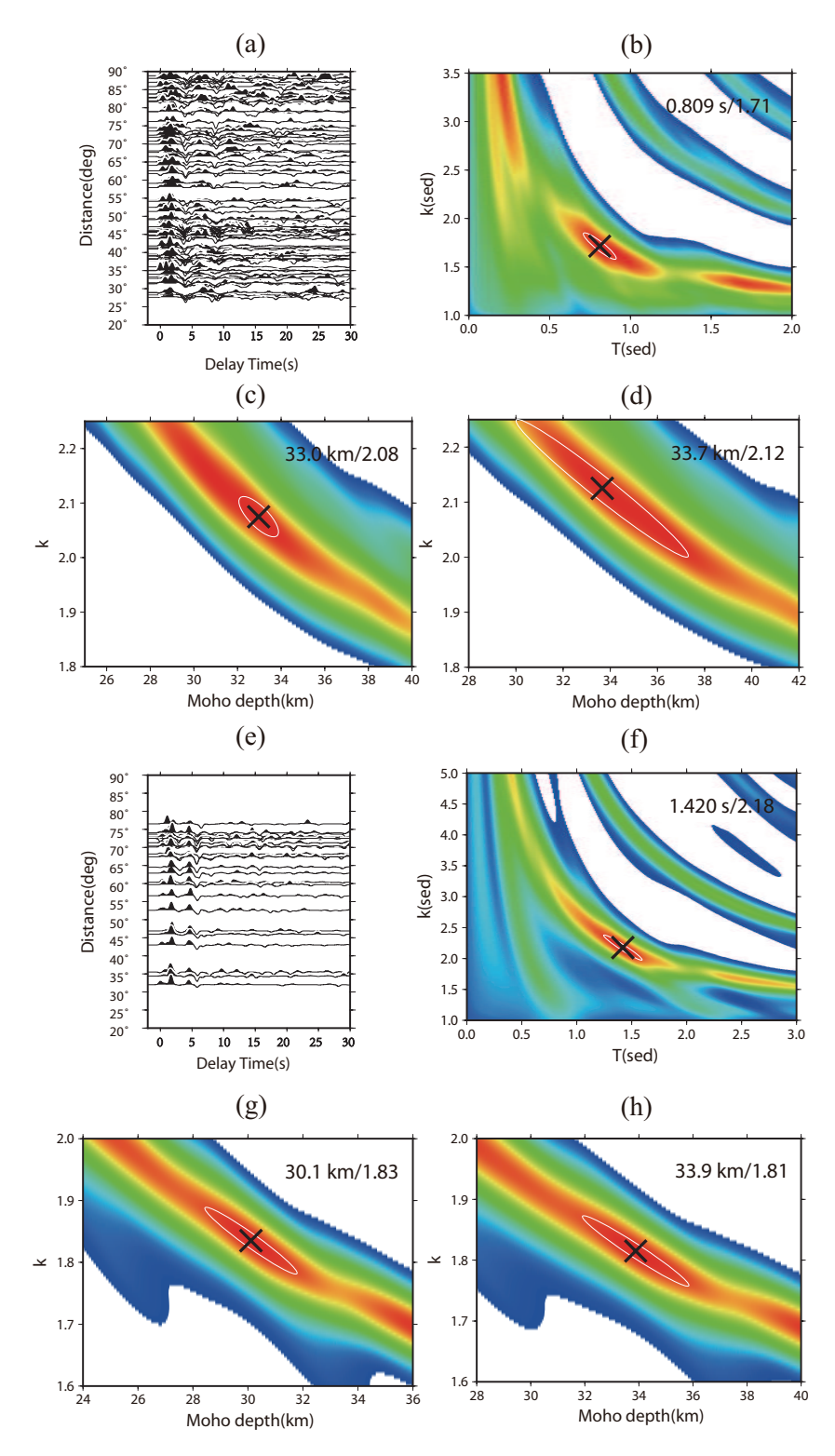


Figure 7: Comparison of the results obtained by using two H-k stacking methods at two typical stations with different sediment thickness. The upper panels show the calculation results of the DZG station, which is located in the Cangxian uplift area where covers thin sediments (location shown in Figure 4). The lower panels show the calculation results of the A003 station, which is located in the Jizhong depression area where covers thick sediments (Figure 4). (a) and (e) are the receiver functions obtained from teleseismic waveform recorded by the two stations. (b) and (f) are the sediment results of the first stack by using the improved sequential H-k stacking method. (c) and (g) are the crustal results of the second stack by using the improved sequential H-k stacking method. (d) and (h) are the results from the H-k stacking method.

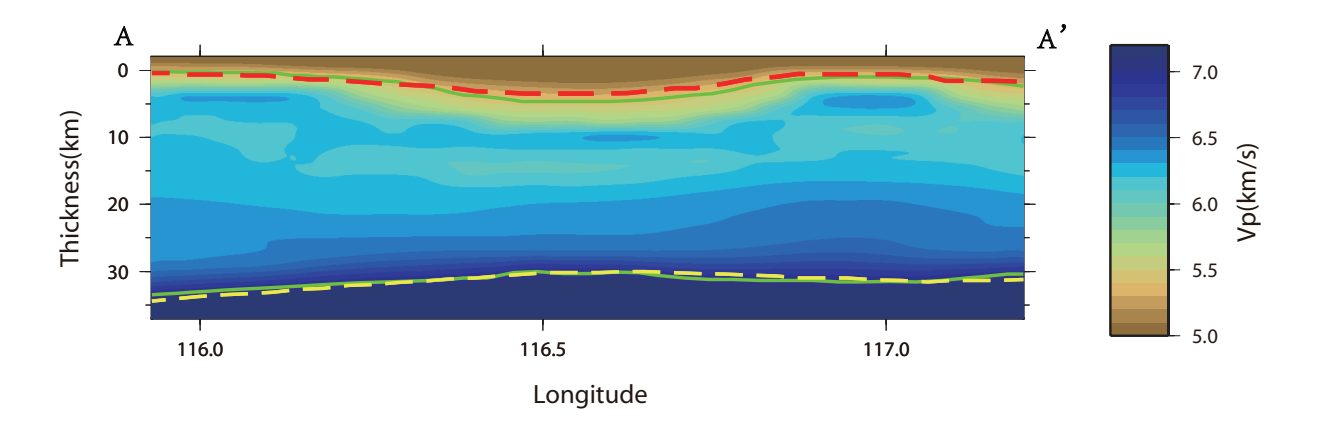


Figure 8: Comparison of the results obtained from the improved method and the DSS profile. The red and yellow dashed lines represent the bottom boundaries of the sediments and the crust obtained by using the improved sequential H-k stacking method. The background colors indicate the P-wave velocity structure from the DSS profile [25]. The P-wave velocity color scale is shown on the right. The two solid green lines represent the bottom boundaries of the sediments and the crust, which are determined by the 5.5 km/s and 7 km/s velocity contours, respectively. The location of the profile is shown in Figure 1.

ancy may be that the stations at  $116.5^{\circ}$  E are not dense (Figure 1).

#### 4.2 Abnormal distribution of the crustal Poisson ratio and discussion of cause

The Poisson ratio is one of the important mechanical parameters which is used to describe rock properties. The Poisson ratio of crust is usually associated with rock and melting degree. In general, the Poisson ratio of felsic acidic rock is less than 0.26, the Poisson ratio of intermediate rock ranges from 0.26-0.28, and the Poisson ratio of mafic basaltic rock ranges from 0.28-0.30. Partial melting can significantly affect the Poisson ratio which increases with increased melting degree. For example, unmelted granite has a Poisson ratio of ~0.24, whereas granite with a 5% melting degree has a higher Poisson ratio of 0.31. In addition, high-pressure, high-temperature experiments indicate that when the Poisson ratio is bigger than 0.3, the crust would most likely be partial melted [29, 30].

Our results show that the Poisson ratio in the study area normally range from 0.23-0.28, but there are two locations with high Poisson ratio (Figure 6). One anomaly is located near the Datong volcano in the western part of the study area, where the Poisson ratio is as high as 0.32. A group of Quaternary volcanoes exists in this area. The most recent volcanic eruption has occurred at approximately 60 ka [31]. Geochemical analyses demonstrate that the mafic volcanic rock is the main erupted component [32]. Thus, the high Poisson ratio can be associated with the mafic magma. The other high Poisson ratio anomaly is

located at the eastern part of the NSGL between Beijing and Yanqing. Zheng *et al.* [33] have reported that the crust-mantle transition zone in this area is relatively thick and the velocity gradient is small, implying the possibility of magma intrusion. The results from body wave tomography also reveal that the Taihangshan Front Fault may cut through the Moho boundary and reach to the upper mantle [26]. Hence, mantle magma may intrude into the lower crust along the weak fault belts, resulting in a higher Poisson ratio in this area.

A significant discrepancy of Poisson ratio is present on the west and east sides of the NSGL. To further analyze the discrepancy, we plot the data (crustal thickness and Poisson ratio) of the west and east parts of the NSGL in Figure 9 with the blue and red dots, respectively. Apparently, the data points of the two regions are mostly separated, indicating that the different features in the two regions are obvious. We utilize regression analysis to the data of two regions. The red and blue lines are the fitted minimum residual lines based on the red and blue data points, respectively. According to Figure 9, the red line is steeper than the blue line, indicating a faster variation of Poisson ratio with the crustal thickness in NCB. In addition, previous studies also suggest that the correlation between thickness and Poisson ratio of crust is closely related to the crustal tectonic activity [34]. The rapid variation of the Poisson ratio with crustal thickness in NCB indicates that complicated geologic evolution has occurred here, the distinct difference of crustal structure in the two areas also reveal that the east part of NCC has experienced more severe destruction and deformation than in the west.

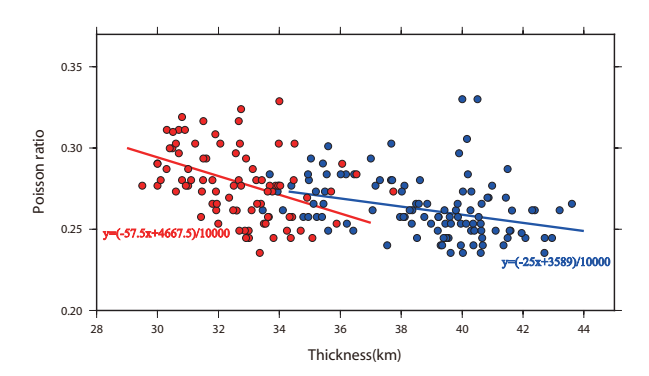


**Figure 9:** Regression analysis of data points in the two regions. The red dots indicate data points on the east of the NSGL, whereas the blue dots represent the data points on the west of the NSGL. The red and blue lines are the fitted minimum residual lines to the data points on the east and west of NSGL, respectively.

Christensen et al. [29] have statistically analyzed the Poisson ratio in the global stable continental cratons and obtained an average value of 0.265. In our study, the average Poisson ratio value on the west part of the NSGL is 0.26, which is similar to the average crustal Poisson ratio in the stable cratons. This result may imply the west part of the NSGL remains stable with a thick crust and gentle variations in Poisson ratio (the blue dots and blue fitted line in Figure 9). In contrast, the Poisson ratio on the east part of the NSGL is relatively high with an average of 0.28, which is possibly associated with the wide extension of the crust in this region [4, 5]. Moreover, Ji et al. [34] have proposed that the main cause of the Poisson ratio discrepancy between the west and east of NSGL can be the different proportions of different rock components in the crust. In the study area, the middle-upper crust is composed of felsic acidic rock with low Poisson ratio, and the lower crust is composed of mafic rock with medium or high Poisson ratio [34]. During crustal extension, the upper crust may have experienced relatively intensive thinning compared to the middle-lower crust. Therefore, the relative proportion of felsic components with low Poisson ratio is reduced, resulting in a high Poisson ratio of the crust in NCB, and Poisson ratio varies with crustal thickness rapidly (the red regression line in Figure 9). In this study, the more accurate results obtained by the improved sequential H-k stacking method reveal the distinct differences of Poisson ratio between the east and the west parts of the NCC. The main reason for this significant difference is the wide crustal extension occurred in the east part of NCC, which may be the crustal response that the destruction and deformation in the east part of NCC are more severe than in the west [1].

#### **5 Conclusions**

Using the H-k stacking method and the improved sequential H-k stacking method proposed in this research, we investigate the structure of the sediments and crust in the northeast NCC. We reach the following conclusions in this study.

- 1. The improved method proposed in this paper needs two sequential stacks. In the first stack, we obtain thickness and the Vp/Vs ratio of sediments with assumption p=0. The Taylor expansion demonstrates that the error resulting from this assumption is small (<0.8%). In the second stack, the thickness and Vp/Vs ratio of crust are calculated based on the sedimentary results. The "recovery tests" of models with velocity jump and velocity gradient in sediments indicate that the errors in the thickness of sediments and crust are less than 1% and 3%, respectively. Through processing actual teleseismic waveform, the results from improved method are similar to results from DSS profiles. Thus, our results demonstrate that in areas with thick sediments, the improved sequential H-k stacking method proposed in this paper can be applied to actual teleseismic data and obtain accurate results.
- 2. The improved method is applied to the NCB and the H-k stacking method is used to the TM and YU. The results show that the sediments in the depressions of NCB are relatively thick, whereas those in the uplifted areas of NCB are thin, identical to the results from the DSS profiles. The crust on the west of the NSGL is thick and has low Poisson ratio. Meanwhile, on the east, the crust is thinner and the Poison ratio is higher. These results and the structural features obtained from the regression analysis demonstrate that the crust of eastern NCC has experienced intensive extension, which may be the crustal response that the destruction and deformation in the east part of NCC are more severe than in the west.

**Acknowledgement:** We thank the Data Management Centre of China National Seismic Network at Institute of Geophysics (SEISDMC, doi:10.11998/SeisDmc/SN), China Earthquake Networks Center and BJ, HE, NM, SX, TJ Seismic Networks, China Earthquake Administration for providing the data of permanent seismic stations, and the North China Seismic Array of IGCEA for providing the data of temporary seismic stations. This research was supported by National Key R&D Plan (Grant No.2017YFC0601406) and NSFC (Grant No.91114205). Plots

were made using the Generic Mapping Tools version 4.2.1 [33] (www.soest.hawaii.edu/gmt; Wessel and Smith 1998).

#### References

- Zhu, R., Xu, Y., Zhu, G., Zhang, H., Xia, Q. and Zheng, T., Destruction of the North China Craton, Science China Earth Sciences, 2012, 55(10), 1565-1587.
- [2] Griffin, W. L., O'Reilly, S. Y. and Ryan, C. G., Composition and thermal structure of the lithosphere beneath South Africa, Siberia and China: proton microprobe studies, In International Symposium on Cenozoic Volcanic rocks and deep-seated xenoliths of China and its Environs, Beijing, 1992, pp. 65-66.
- [3] Griffin, W. L., Zhang, A. D., O'Reilly, S. Y. and Ryan, C. G., Phanerozoic evolution of the lithosphere beneath the Sino-Korean craton, Mantle dynamics and plate interactions in East Asia, Am. Geophy. Union, Washington, D. C., Geodyn. Ser., 1998, 27, 107-126.
- [4] Menzies, M. A., Fan, W. and Zhang, M., Palaeozoic and Cenozoic lithoprobes and the loss of> 120 km of Archaean lithosphere, Sino-Korean craton, China. Geological Society, London, Special Publications, 1993, 76(1), 71-81.
- [5] Menzies, M. A. and Xu, Y., Geodynamics of the North China Craton. In Mantle Dynamics and Plate Interactions in East Asia, Am. Geophy. Union, Washington, D. C., Geodyn. Ser., 1998, 27, 155-165
- [6] Vinnik, L.P., Detection of waves converted from P to SV in the mantle, Phys. Earth Planet. Inter., 1977, 15, 39-45.
- [7] Langston, C.A., Structure under mount rainer, washington, inferred from teleseismic body waves, J. Geophys. Res., 1979, 84(B9), 4749-4762.
- [8] Owens, T.J., Zandt, G. and Taylor, S.R., Seismic evidence for an ancient rift beneath the cumberland plateau, Tennessee: A detailed analysis of broadband teleseismic P waveforms, J. Geophys. Res., 1984, 89, 7783-7796.
- [9] Zhu, L. and Kanamori, H., Moho depth variation in southern California from teleseismic receiver functions, J. Geophys. Res. Solid Earth (1978–2012), 2000, 105(B2), 2969-2980.
- [10] Xu, W. and Zheng, T., Distribution of Poisson's ratios in the northwestern basin-mountain boundary of the Bohai Bay Basin, Chinese J. Geophys., 2005, 48(5):1077-1084 (in Chinese).
- [11] Wang, J., Liu Q., Chen J., Li S., Guo B. and Li X., The crustal thickness and Poisson's ratio beneath the Capital Circle Region, Chinese J. Geophys., 2009, 52(1):57-66 (in Chinese).
- [12] Chen, L., Zheng, T. and Xu, W., Receiver function migration image of the deep structure in the Bohai Bay Basin, eastern China. Geophys. Res. Lett., 2006, 33(20):129-143. https://doi.org/10.1029/2006GL027593.
- [13] Tang, C., Chen, C, and Teng T., Receiver Functions for Three-layer Media, Pure Appl. Geophys., 2008, 165,1249-1262.
- [14] Wei, Z., Chen L., Li Z., Ling Y. and Li J., Regional variation in Moho depth and Poisson's ratio beneath eastern China and its tectonic implications, J. Asian Earth Sci., 2016, 115, 308-320.
- [15] Kennett, B.L.N., The removal of free surface interactions from three-component seismograms. Geophy. J. Int., 1991, 104(1), 153-163.

- [16] William, L. Yeck. Anne F. Sheehan. and Vera Schulte-Pelkum., Sequential H-k Stacking to Obtain Accurate Crustal Thicknesses beneath Sedimentary Basins, Bull. Seismol. Soc. Am., 2013, 103(3), 2142-2150.
- [17] Tao, K., Liu, T., Ning, J. and Niu, F., Estimating sedimentary and crustal structure using wavefield continuation: theory, techniques and applications, Geophys. J. Inter., 2014, 197(1):443-457, https://doi.org/10.1093/gji/ggt515.
- [18] Yu, Y., Song, J., Liu, L. and Gao S., Determining crustal structure beneath seismic stations overlying a low-velocity sedimentary layer using receiver functions, J. Geophys. Res. Solid Earth, 2015. 120, 3208–3218.
- [19] Zheng, X., Yao, Z., Liang, J. and Zheng, J., The role played and opportunities provided by IGP DMC of China National Seismic Network in Wenchuan earthquake disaster relief and researches, Bull. Seismol. Soc. Am., 2010, 100(5B), 2866~2872.
- [20] Ligorria, J. P. and Ammon, C. J., Iterative deconvolution and receiver-function estimation, Bull. Seismol. Soc. Am., 1999, 89, 1395-1400
- [21] Niu, F., Alan, L., Sangwon, H. and Masayuki, O., Mapping the subducting Pacific slab beneath southwest Japan with Hi-net receiver functions, Earth Planet. Sci. Lett., 2005, 239, 9-17.
- [22] Herrmann, R. B., Computer programs in seismology: An evolving tool for instruction and research, Seism. Res. Lettr., 2013, 84, 1081-1088. doi:10.1785/0220110096.
- [23] Yang, F. and Huang, J., High precision 3D P-wave velocity model of the upper crust under the Chinese capital region based on oil seismic stack velocity and deep seismic sounding, Chinese J. Geophys., 2013, 56(5):1487-1496 (in Chinese).
- [24] He, C., Zhu, L., Ding, Z. and Pan, J., Sedimentary Cover in the Bohai Basin using Teleseismic Receiver function, Acta Geologica Sinica, 2010, 84(5), 716-722 (in Chinese).
- [25] Jia, S., Qi, C., Wang, F., Chen, Q., Zhang, X. and Chen, Y., Three-Dimensional Crustal Gridded Structure of the Capital Area, Chinese J. Geophys., 2005, 48(6), 1397-1407 (in Chinese).
- [26] Huang, J. and Zhao, D., Crustal heterogeneity and seismotectonics of the region around Beijing, China, Tectonophysics, 2004, 385(1), 159-180.
- [27] Jia, S., Wang, F., Tian, X., Duan, Y., Zhang, J., Liu, B. and Lin, J., Crustal structure and tectonic study of North China Craton from a long deep seismic sounding profile, Tectonophysics, 2014, 627, 48-56.
- [28] Deng, Y., Fan, W., Zhang, Z. and Liang, K. The gravity and isostatic Moho in North China Craton and their implications to seismicity, Earthq. Sci., 2014, 27(2), 197-207.
- [29] Christensen, N. I., Poisson's ratio and crustal seismology, J. Geophys. Res., 1996, 101, 3139-3156.
- [30] Zandt, G. and Ammon, C. J., Continental crust composition constrained by measurements of crustal Poisson s ration, Nature, 1995, 374, 152-154.
- [31] Liu, J., Han. J. and William, S., Cenozoic episodic volcanism and continental rifting in northeast China and possible link to Japan Sea development as revealed from K-Ar geochronology, Tectonophysics, 2001, 339, 385-401.
- [32] Ma, J. and Xu, Y., Petrology and geochemistry of the Cenozoic basalts from Yangyuan of Hebei Province and Datong of Shanxi Province: Implications for the deep process in the western North China Craton, Geochimica, 2004, 33(1), 75-88 (in Chinese).
- [33] Zheng, T., Chen, L., Zhao, L., Xu, W. and Zhu, R., Crustmantle structure difference across the gravity gradient zone in

- North China Craton: seismic image of the thinned continental crust, Phys. Earth Planet. Inter., 2006, 159(1), 43-58.
- [34] Ji. S., Wang, Q. and Yang, W., Correlation between Crustal Thickness and Poisson's Ratio in the North China Craton and Its Implication for Lithospheric Thinning, Acta Geologica Sinica, 2009, 83(3), 324-329 (in Chinese).